Quaternary Research 71 (2009) 227–238

Contents lists available at ScienceDirect

Quaternary Research

journal homepage: www.elsevier.com/locate/yqres

Long-term and short-term vertical velocity profiles across the forearc in the NE Japan subduction zone

Tabito Matsu'ura [a,*], Akira Furusawa [b], Hidetaka Saomoto [c]

[a] Active Fault Research Center, AIST, GSJ, Site 7, 1-1-1 Higashi, Tsukuba, Ibaraki 305-8567, Japan
[b] Furusawa Geological Survey, Japan
[c] Toyota Central R & D Laboratories, Inc., Japan

ARTICLE INFO

Article history:
Received 22 August 2007
Available online 25 January 2009

Keywords:
Late Quaternary
Northeast Japan
Marine terrace
Uplift rate
GPS
Vertical velocity profile

ABSTRACT

We estimated the long-term vertical velocity profile across the northeastern Japan forearc by using the height distribution of late Quaternary marine and fluvial terraces, and we correlated the ages of the two marine terraces with marine isotope stages (MIS) 5.5 and 5.3 or 5.1 by cryptotephra stratigraphy. The uplift rate, estimated as 0.11–0.19 m ka^{-1} from the relative heights between the terrace surfaces and eustatic sea levels, was nearly equal to, or slightly slower than, the uplift rate farther inland (0.15–0.19 m ka^{-1}), as determined from the relative heights of fill terrace surfaces. In contrast, the short-term vertical velocity profile, obtained from GPS observations, showed that the forearc is currently subsiding at a maximum rate of 5.4±0.4 mm yr^{-1}. Thus, the current short-term (geodetic) subsidence does not reflect long-term (geological) tectonic movement. Short-term vertical deformation is probably driven by subduction erosion or elastic deformation caused by interplate coupling, or both. However, long-term uplift is probably due not to moment release on the mega-thrust but to crustal thickening.

Introduction

Moment release on a mega-thrust in a subduction zone usually warps the crust of the overriding plate to build the forearc high (non-volcanic mountains). Vertical deformation of the forearc during both coseismic and postseismic periods has been monitored in the southwestern Japan subduction zone (Fitch and Scholz, 1971; Savage and Thatcher, 1992; Hyndman and Wang, 1995), the Aleutian subduction zone (Plafker, 1972; Zong et al., 2003), and the Peru–Chile subduction zone (Plafker, 1972), and in each case both along-trench coseismic subsidence (or uplift) and postseismic uplift (or subsidence) occurred. A similar pattern of deformation has probably also occurred in the Cascadia subduction zone, as inferred from a dislocation model (Satake et al., 2003; Wang et al., 2003).

Information about these vertical deformations covers a time period that is too short (10^0–10^1 yr) to discuss the long-term plate deformation responsible for mountain-building. In contrast, marine and fluvial terrace surfaces are widely used as indicators of long-term (10^2–10^6 yr) forearc deformation. Marine terrace surfaces (paleo-shorelines) have been studied to show the dynamics of late Quaternary uplift in, for example, the southwestern Japan (Yoshikawa et al., 1964; Maemoku and Tsubono, 1990) and Aleutian (Plafker, 1987) subduction zones. Furthermore, fluvial terrace surfaces (uplifted alluvial surfaces) have also been studied to show the dynamics of late Quaternary uplift in the Cascadia subduction zone (Pazzaglia and Brandon, 2001).

All of these studies, however, were conducted in accretion-dominant subduction zones. Vertical deformation in northeastern Japan (NE Japan) is unusual, because it is occurring in the erosion-dominant NE Japan subduction zone (Fig. 1A: Matsu'ura et al., 2008). Short-term deformation revealed by GPS observation shows subsidence in the southern part of the NE Japan forearc (Fig. 1B: Suwa et al., 2006), which is consistent with the present "rias" coast (a typical submergence coast), and Heki (2004a) has suggested that subsidence in NE Japan has been driven by basal tectonic erosion since 16 Ma. In contrast, terrace surfaces occurring intermittently along the coast (Miura, 1966) may indicate uplift (Koike and Machida, 2001), which is not consistent with continuous basal tectonic erosion since 16 Ma. Therefore, the mechanism of the forearc uplift must be revised to explain both the short-term (geodetic) subsidence and the long-term (geological) uplift. However, to date, the nature of the terrace surfaces, whether marine or fluvial, has yet to be clarified, and the ages of the terraces are also unknown.

We studied the late Quaternary (permanent) deformation rate of the NE Japan forearc in the NE Japan subduction zone. We first investigated the ages of the terraces along the Pacific coast (Kesennuma Bay) by using tephrostratigraphy, and we estimated the long-term uplift rate from the relative heights between the terrace surfaces and eustatic sea levels. Next, we compiled GPS data to obtain the interseismic velocity of the vertical tectonic movement of the NE

* Corresponding author. Fax: +81 29 852 3461.
E-mail address: matsuura-t@aist.go.jp (T. Matsu'ura).

0033-5894/$ – see front matter © 2008 University of Washington. All rights reserved.
doi:10.1016/j.yqres.2008.12.005

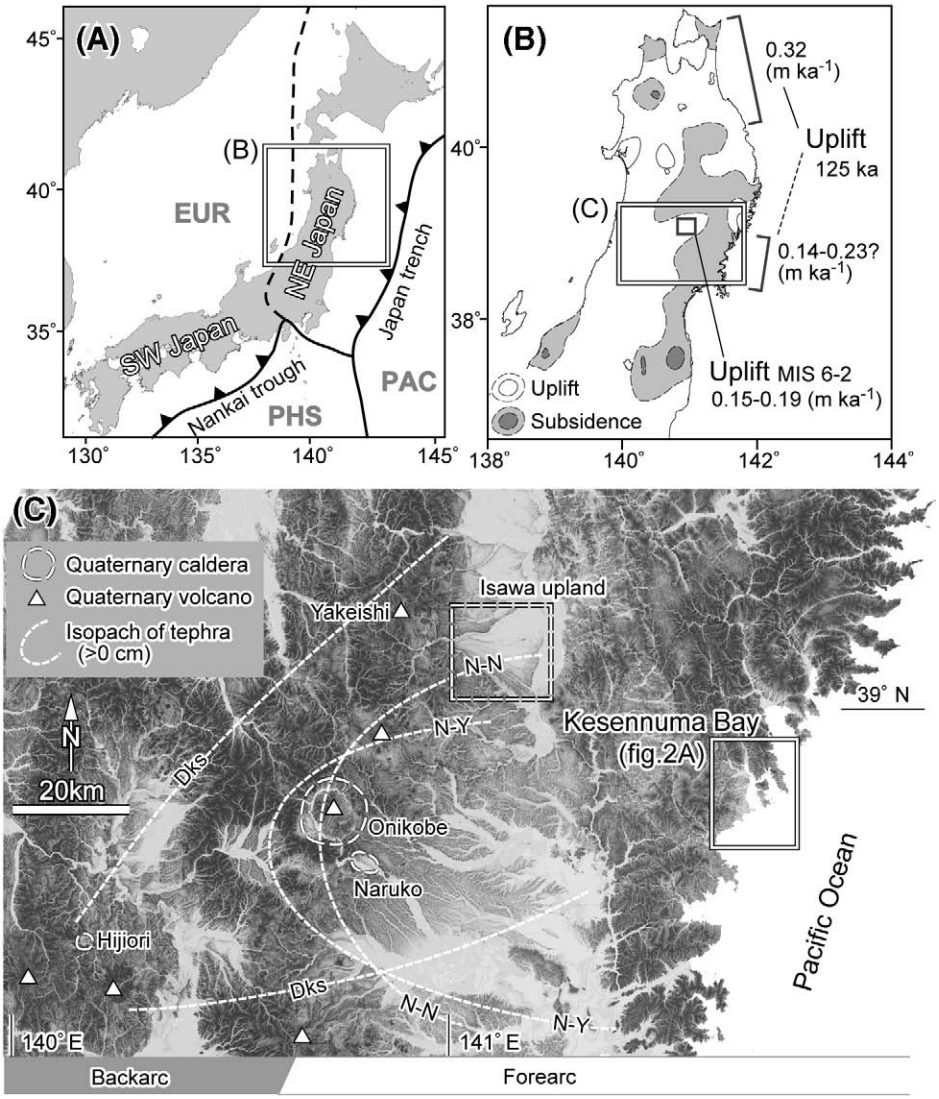

Figure 1. Tectonic setting showing vertical velocities in northeastern (NE) Japan and the study area (Kesennuma Bay). (A) Tectonic setting of the NE Japan arc. The Pacific plate (PAC) and the Philippine Sea plate (PHS) are subducting under the Eurasian plate (EUR). The NE Japan arc is in the subduction zone between the Pacific and Eurasian plates. (B) Vertical velocities estimated from GPS data and marine terraces. The vertical deformation pattern is from GPS data for 1997–2001 (Suwa et al., 2006). The contour interval is 5 mm yr^{-1}. Uplift rates inferred from the height of the MIS 5.5 marine terrace surface (125 ka) are from Koike and Machida (2001), but marine terraces in the southern part of the NE Japan forearc do not have any age constraints. Uplift rates inferred from the relative height between MIS 6 and MIS 2 fluvial terraces are from Matsu'ura et al. (2008). (C) Map showing the location of Kesennuma Bay in the NE Japan forearc. Tephra abbreviations: Dks, Dokusawa (90–100 ka); N-N, Naruko-Nisaka (90–100 ka); N-Y: Naruko-Yanagisawa (41–63 ka). Isopachs of Dks are from Matsu'ura et al. (2002), and those of N-N and N-Y are from Machida and Arai (2003). The map image is from Yokoyama et al. (2002).

Japan forearc. Finally, we reconstructed the vertical velocity profile across NE Japan from late Quaternary marine and fluvial terrace surfaces. On the basis of our results, we propose here a novel mechanism (long-term isostatic uplift driven by crustal thickening and short-term elastic deformation) to explain the long-term uplift and short-term subsidence in this erosion-dominant subduction zone.

Regional setting of Kesennuma Bay

Kesennuma Bay is on the Pacific coast of Japan in the NE Japan forearc (Fig. 1C). The shoreline around Kesennuma Bay is a typical rias coast, which is generally interpreted as a submergent coast. Recent GPS data also show subsidence at a maximum rate of 5 mm yr^{-1} in the NE Japan forearc (Fig. 1B: Aoki and Scholz, 2003; Suwa et al., 2006). During the Quaternary, however, the Kesennuma area experienced uplift, as shown by multiple levels of terrace surfaces (Fig. 2). These terrace surfaces are overlain by (middle to) late Pleistocene loess, which varies in thickness (<1 m; Fig. 3). The loess deposits do not include any visible tephras, but they do contain cryptotephras (volcanic ash horizons that cannot be discerned with the naked eye in sedimentary sequences), as shown by isopach maps of several late Pleistocene tephras indicating that these tephras cover Kesennuma Bay (Fig. 1C). These cryptotephras can be used to constrain the ages of the late Quaternary terrace surfaces. There are no known active Quaternary faults around Kesennuma Bay (Research Group for Active Faults of Japan, 1991).

Methods

We classified the terraces in the study area by interpretation of aerial photographs, distinguishing and mapping the terrace surfaces on 1:5000 or 1:25,000 scale topographic maps with 2- or 5-m contour intervals, and constructed a profile of each terrace surface from the topographic map contours. We determined the ages of the terrace surfaces on the basis of tephrostratigraphy and used them to correlate the terrace surfaces with marine isotope stages (MIS). We calculated rates of uplift from elevation differences between dated marine terrace surfaces and eustatic sea level.

https://doi.org/10.1016/j.yqres.2008.12.005 Published online by Cambridge University Press

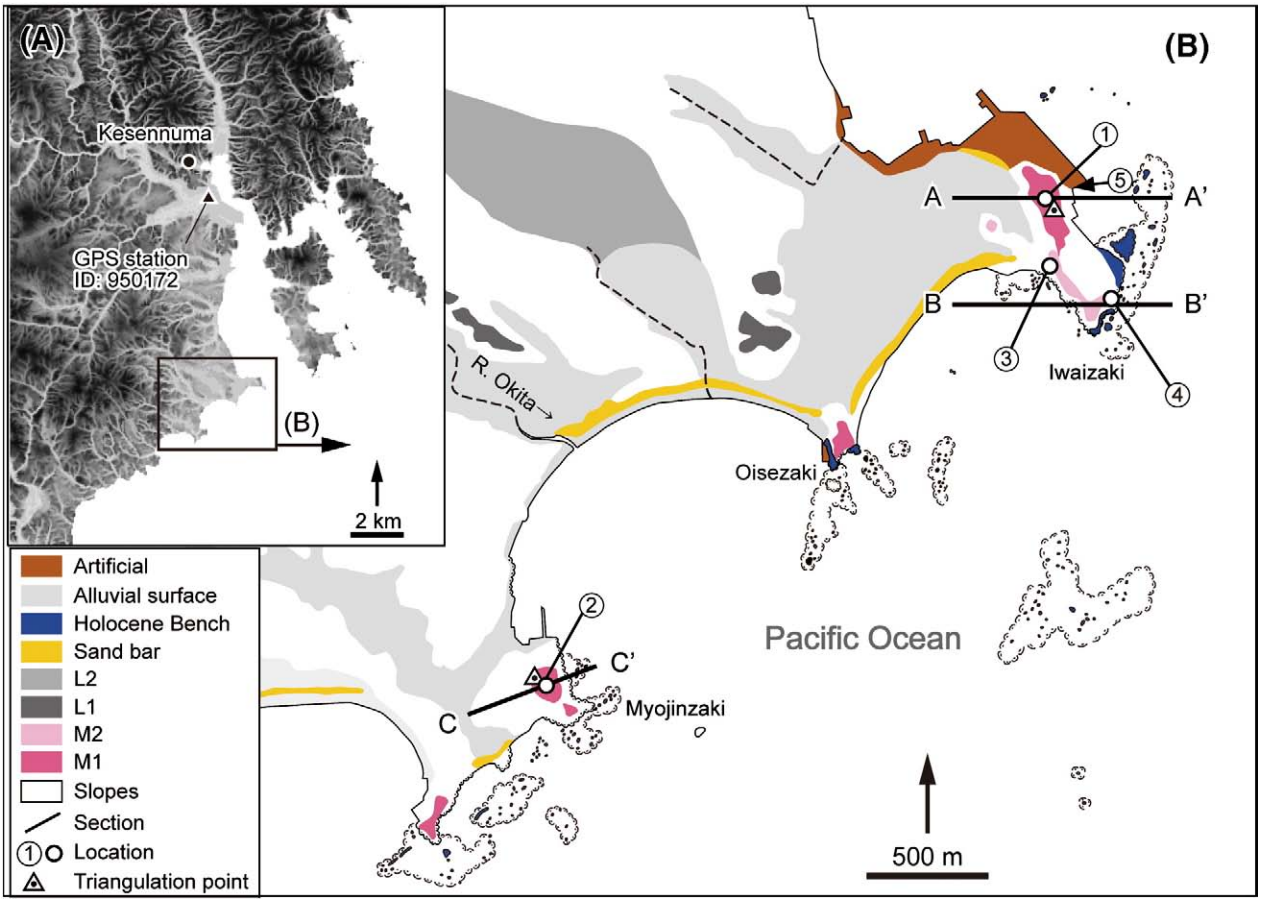

Figure 2. Maps showing the distribution of terraces in Kesennuma Bay and sampling locations. (A) Map showing the location of the study area. The location of the GPS station (ID: 950172) is also shown. (B) Map showing the distribution of the terrace surfaces. Sampling and cross section locations and triangulation points (maintained by GSI) are also shown.

For tephra identification, we sampled reported tephras that cover the study area shown by isopach maps, and we obtained samples of the loess deposits (including cryptotephras) on terraces by boring. Contiguous samples from cores were sieved under running water through disposable 0.125-mm and 0.0625-mm sieves. The disposable sieves were changed between samples to prevent contamination. The residues were dried, embedded in resin and mounted on slides for examination of the grain composition. For the optical analyses, about 15 heavy mineral (orthopyroxene and amphibole) grains were picked from each sample. Refractive indices of heavy minerals (orthopyroxene, gamma; amphibole, n_2) were analyzed by the MAIOT system (Furusawa, 1995). For the geochemical analyses, about 15 glass shards were picked from each sample. The major chemical composition of the glass shards was analyzed by using an electron microprobe system (energy-dispersive spectrometry: HORIBA EMAX 5770 or HORIBA EMAX ENERGY EX-250). Eight major elements were measured with a counting time of 200 s. All elements are expressed as weight percent. An accelerating voltage of 15 kV and a beam strength of 0.3 nA with beam diameter of 150 nm were used for scanning a 4-μm grid of the targeted glass shard. The ZAF procedure was applied to correct for the atomic number effect.

We used a GPS data series acquired by the Geographical Survey Institute (GSI) of Japan to determine the rates of short-term vertical deformation. GSI operates a nationwide GPS network, GEONET (GPS Observation Network System), to monitor regional crustal deformation (Hatanaka et al., 2003). The GPS station coordinates are referenced to the International Terrestrial Reference Frame 2000 (Altamimi et al., 2002). We determined the vertical deformation rate at each GPS station from the gradient of the least-squares-fitted line between station height and time. The standard error (99% confidence interval) of each vertical deformation rate was also calculated.

Correlations of tephras

Dokusawa tephra (Dks)

The Dokusawa tephra (Dks) erupted from the backarc (from the Hijiori volcano or another volcano in its vicinity; Fig. 1C; Matsu'ura et al., 2002, 2003). The Dks sample for chemical analysis is obtained from a type location (38.6564°N, 140.3194°E; Matsu'ura et al., 2002). Dks shards have high K_2O (>3.5 wt.%; Fig. 4) because the source volcano is far from the volcanic front. This high-K glass is unusual in the forearc, where low-K (<2 wt.%) volcanic glass shards are dominant. The heavy mineral assemblage of Dks consists of cummingtonite and biotite, with minor amounts of hornblende and orthopyroxene. The refractive indices of the cummingtonite (n_2) range from 1.666 to 1.671. The eruptive age of Dks is MIS 5.2–5.3, on the basis of its stratigraphic relationship with the Ontake-Pm1 tephra (MIS 5.3) and the Aso-4 tephra (MIS 5.2–5.1; Machida and Arai, 2003).

Naruko-Nisaka tephra (N-N)

The Naruko-Nisaka tephra (N-N) erupted from the Naruko caldera (Fig. 1C: Soda, 1989). The N-N sample for chemical analysis is obtained from an outcrop shown by Soda (1996; 38.6733°N, 140.9017°E). N-N shards, which have low K (1.6–1.8 wt.%), are distinguishable by their K content from Dks glass shards (Fig. 4). The heavy mineral assemblage consists of orthopyroxene with minor amounts of hornblende, cummingtonite and biotite. The refractive indices of the orthopyroxene

https://doi.org/10.1016/j.yqres.2008.12.005 Published online by Cambridge University Press

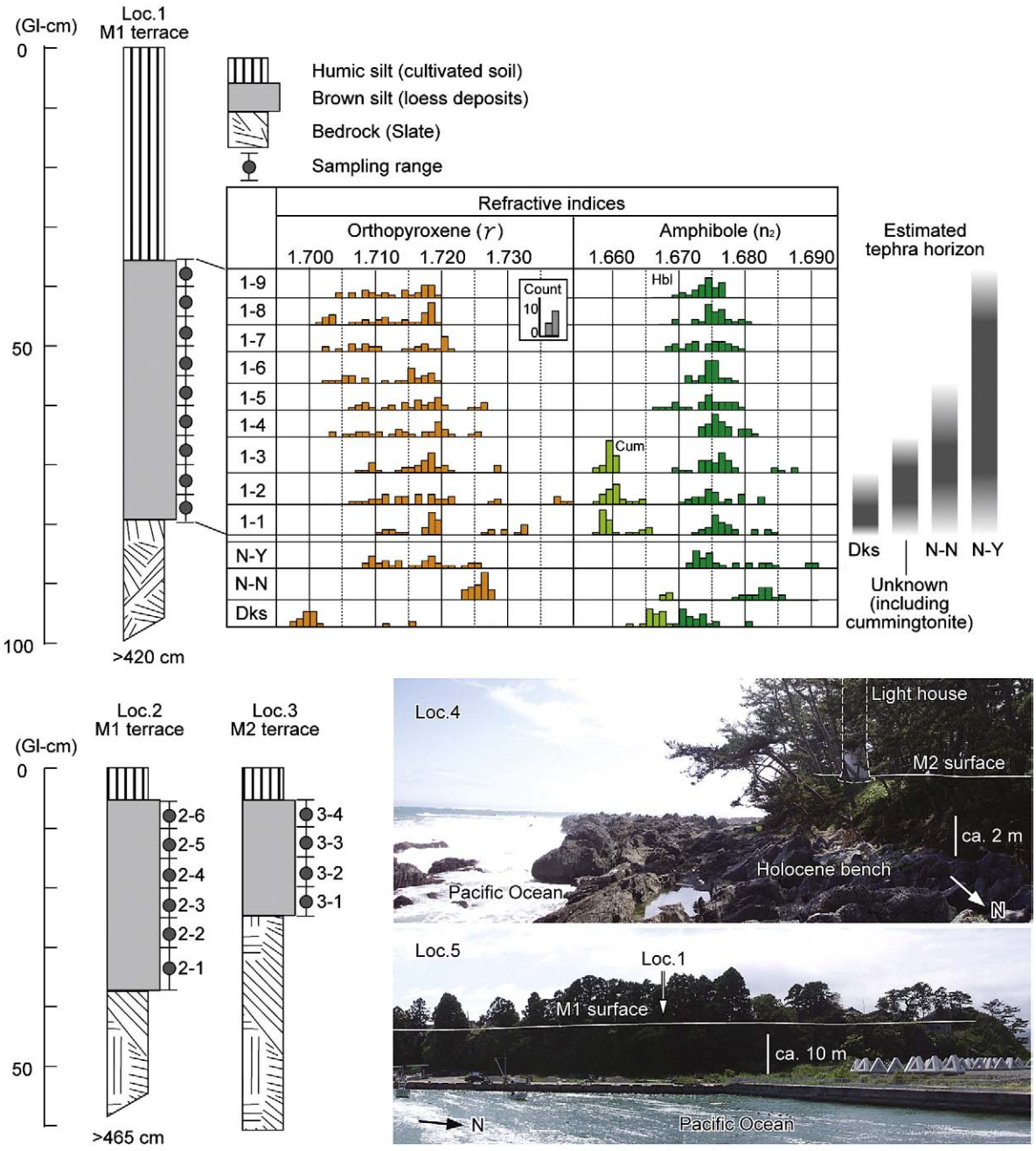

Figure 3. Geological columns with refractive indices of cryptotephras and photos of terraces. Tephra abbreviations are explained in Figure 3. Refractive indices were determined by the MAIOT system (Furusawa, 1995). The amphiboles (n_2) are cummingtonite (Cum) and hornblende (Hbl).

(γ) range from 1.723 to 1.728, those of the cummingtonite (n_2) from 1.667 to 1.669, and those of the hornblende (n_2) from 1.678 to 1.686. The eruptive age of N-N is MIS 5.2–5.3, on the basis of its stratigraphic relationship with the Ontake-Pumice 1 tephra and the Aso-4 tephra (Machida and Arai, 2003).

Naruko-Yanagisawa (N-Y)

The Naruko-Yanagisawa tephra (N-Y) erupted from the Naruko caldera (Fig. 1C: Soda, 1989). The N-Y sample for chemical analysis is obtained from an outcrop shown by Tsuchiya et al. (1997; 38.7361°N, 140.8236°E). N-Y shards have low K (1.6–1.8 wt.%) and are also distinguished from Dks shards by their K content (Fig. 4). Moreover, N-Y shards have lower CaO content and higher Na_2O content than N-N shards. The N-Y heavy mineral assemblage consists of orthopyroxene with minor amounts of hornblende and biotite. The refractive indices of the orthopyroxene (γ) and hornblende (n_2) range from 1.708 to 1.726 and 1.671 to 1.691, respectively. The eruptive age of N-Y is 41–63 ka, on the basis of ^{14}C, thermoluminescence and fission-track dating (Machida and Arai, 2003) and the age is correlated to MIS 4.

Cryptotephras at Kesennuma Bay and its correlations

The loess deposits at locs. 1 and 2 on terrace surfaces were sampled by rotary coring (core diameter 66 mm). From each core, contiguous samples were obtained, each about 5 cm thick (Fig. 3; Table 1). The deposits do not include any visible tephras but do include fresh volcanic glass shards and minerals. Core samples 1–1 to 1–9 (from loc. 1) and samples 2–1 to 2–6 (from loc. 2) contained glass shards (0.9%–14.5% and 0.3%–19.3%, respectively), orthopyroxene (0.1%–1.5% and

https://doi.org/10.1016/j.yqres.2008.12.005 Published online by Cambridge University Press

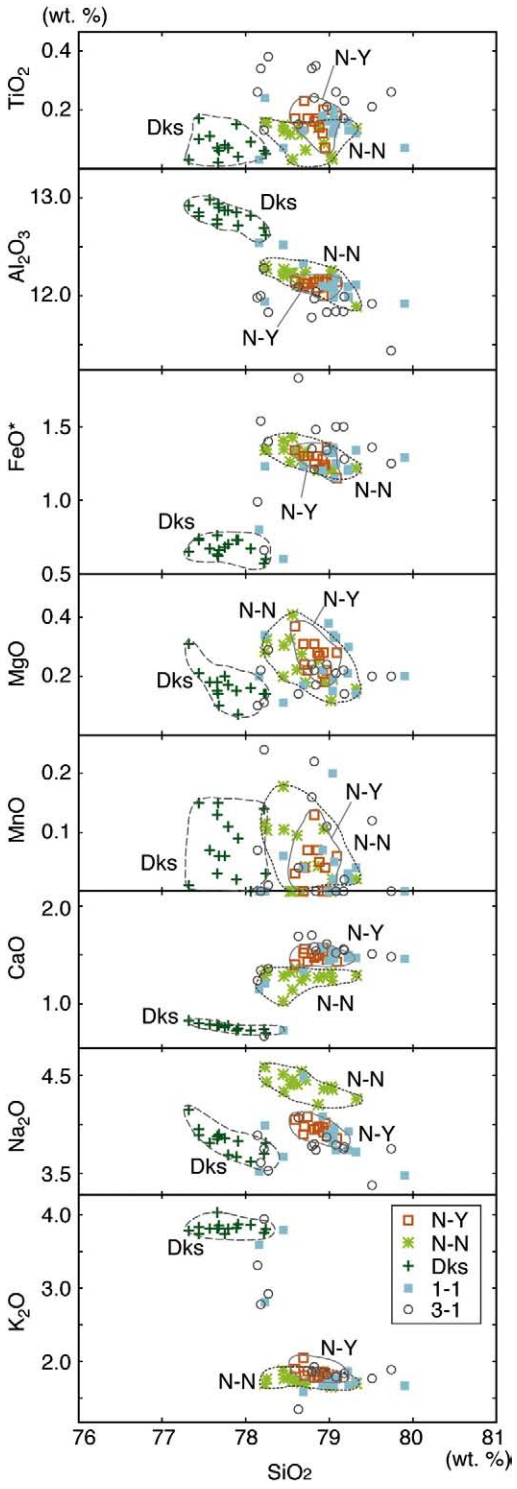

Figure 4. Chemical compositions of volcanic glass shards determined by electron probe micro analysis. Glass shards from samples 3–1 were analyzed by using a HORIBA EMAX ENERGY EX-250 Energy Dispersive X-Ray Micro Analyzer, and the others were analyzed by using a HORIBA EMAX 5770 Energy Dispersive X-Ray Micro Analyzer.

0.3%–1.7%, respectively), and hornblende (0.4%–2.8% and 0.1%–1.7%, respectively). Trace amounts of cummingtonite and biotite were present at both locations (Table 1). Glass shards, orthopyroxene, and hornblende increase upward similarly in core samples from loc. 1 and loc. 2, indicating that at these locations the cryptotephra stratigraphy is probably the same. Thus, we used core samples from loc. 1 for all analyses of refractive indices and chemical composition because the loess deposits there were slightly thicker than at loc. 2.

The refractive indices of orthopyroxene (γ) and hornblende (n_2) ranged from 1.701 to 1.740 (most from 1.706 to 1.720) and 1.661 to 1.688 (most from 1.671 to 1.679), respectively. These ranges overlap those of N-Y and imply the loess deposits include N-Y as a cryptotephra. The orthopyroxene refractive indices (γ) of samples 1–1 to 1–5 show an intermittent distribution between 1.724 and 1.740. These overlap those of N-N and the loess deposits include N-N as a cryptotephra. The refractive indices of cummingtonite (n_2) are distributed bimodally, from 1.657 to 1.661 and from 1.661 to 1.666 at 65–80 cm depth (samples 1–1 to 1–3). The higher range overlaps the distribution of Dks and this implies the loess deposits include Dks as a cryptotephra.

The volcanic glass shards of sample 1–1 can be divided into three populations by K_2O content (Fig. 4). Glass shards containing 3.6–3.8% K_2O (high-K glass) plot on the Dks population. Glass shards containing 1.6–1.9% K_2O (low-K glass) are abundant in the samples and they plot on the N-N and N-Y populations. The low-K glass shards can be further divided into two groups on the basis of their CaO content: high-Ca glass (1.4–1.6%) and low-Ca glass (1.1–1.3%). The high-Ca and the low-Ca glass shards from sample 1–1 plot to the N-Y and N-N populations, respectively. The sources of glass shards containing about 2.8% K_2O (middle-K glass) are indeterminate.

Thus, refractive indices of minerals and chemical compositions of the volcanic glass shards show that the loess deposits at loc. 1 include Dks, N-N and N-Y as cryptotephras (Fig. 3).

The loess deposits at loc. 3 on the terrace surface were sampled with a soil sampler. The contiguous samples (sample diameter 13 mm) were each 5 cm thick (Fig. 3; Table 1). The deposits also include fresh volcanic glass shards and minerals (Fig. 3; Table 1). Core samples 3–1 to 3–4 (loc. 3) contained glass shards (0.5–3.1%), orthopyroxene (0.1–0.6%), hornblende (0.1–0.7%), and trace amounts of cummingtonite and biotite (Table 1). The refractive indices of orthopyroxene (γ) and hornblende (n_2) from sample 3–1 to 3–4 ranged 1.697 to 1.736 (most from 1.704 to 1.721) and 1.668 to 1.686 (most from 1.672 to 1.680), respectively. These are similar to those of N-Y.

The volcanic glass shards of sample 3–1 can be divided into three populations by K_2O content (Fig. 4). A glass shard containing 3.9% K_2O (high-K glass) plotted with the Dks population, but a glass shard containing 12.3% Al_2O_3 did not plot with the DKs population. Glass shards containing 1.8–1.9% K_2O (low-K glass) were abundant in the samples, and they plotted with the N-N and N-Y populations. The low-K glass shards with high-Ca content (1.5–1.7%) plotted with the N-Y population. The sources of the glass shards containing 2.7–3.1% K_2O (middle-K glass) could not be determined.

Thus, the loess deposits at loc. 3 include N-Y as a cryptotephra. Dks and N-N horizons were not observed in the loess deposits at loc. 3.

Sequences and ages of the terrace surfaces

In the study area, multiple levels of fluvial and marine terraces are found (Fig. 2). On the basis of aerial photo interpretation and tephrostratigraphy, we classified the terraces into middle (M1, M2) and lower (L1, L2) surfaces, in descending order. Location 1 is on the M1 terrace surface and is near a triangulation point (elevation: 15.5 m) maintained by GSI at Iwaizaki. Location 2 is on the M1 terrace surface and is near a triangulation point (elevation: 19.9 m) maintained by GSI at Myojinzaki. Locations 3 and 4 are on the M2 terrace surface at Iwaizaki.

The M1 terrace surface is intermittent in the study area and generally well preserved (Fig. 3; a photo of the M1 terrace surface is taken from loc. 5). It originated as a wave-cut bench because there are no marine deposits on the bedrock at locs. 1 or 2 (Fig. 3). The M1 terrace surface is overlain by loess deposits <50 cm thick containing Dks, N-N, and N-Y cryptotephras, in descending order. The M1 terrace surface (a marine terrace surface) must thus be slightly older than MIS 5.2–5.3, MIS 5.5 (122 ka; Bassinot et al., 1994: Table 2), because Dks

https://doi.org/10.1016/j.yqres.2008.12.005 Published online by Cambridge University Press

Table 1
Glass shard content and mineral assemblages in the loess deposits

Location	Sample	Depth (cm)	Glass and mineral assemblage (%)				
			Glass shards	Orthopyroxene	Hornblende	Cummingtonite	Biotite
Loc. 1	1–9	35–40	11.6	1.1	2.0	Trace	Trace
Loc. 1	1–8	40–45	13.6	1.5	2.2	Trace	Trace
Loc. 1	1–7	45–50	13.4	1.2	1.0	Trace	Trace
Loc. 1	1–6	50–55	14.5	1.0	2.8	Trace	Trace
Loc. 1	1–5	55–60	14.5	0.9	1.9	Trace	Trace
Loc. 1	1–4	60–65	13.2	0.9	1.6	Trace	Trace
Loc. 1	1–3	65–70	4.5	0.6	0.6	Trace	Trace
Loc. 1	1–2	70–75	0.9	0.2	0.6	Trace	Trace
Loc. 1	1–1	75–80	0.9	0.1	0.4	Trace	Trace
Loc. 2	2–6	5–10	14.7	1.7	1.7	Trace	Trace
Loc. 2	2–5	10–15	19.3	1.4	1.2	Trace	Trace
Loc. 2	2–4	15–20	14.6	0.9	0.8	Trace	Trace
Loc. 2	2–3	20–25	13.6	0.5	0.7	Trace	Trace
Loc. 2	2–2	25–30	1.5	0.5	0.2	Trace	Trace
Loc. 2	2–1	30–37	0.3	0.3	0.1	Trace	Trace
Loc. 3	3–4	5–10	2.5	0.4	0.5	Trace	Trace
Loc. 3	3–3	10–15	3.1	0.6	0.7	Trace	Trace
Loc. 3	3–2	15–20	2.0	0.3	0.6	Trace	Trace
Loc. 3	3–1	20–25	0.5	0.1	0.1	Trace	Trace

dates to MIS 5.2–5.3 (Matsu'ura et al., 2002). Because we observed no loess deposits correlated with MIS 5.4 between the Dks cryptotephra and the M1 terrace surface at loc. 1, it is uncertain whether the loess deposits on the M1 terrace accumulated immediately after stabilization of the terrace surface.

The M2 terrace surface is found only at Iwaizaki (Fig. 2). This terrace also originated as a wave-cut bench, because marine deposits are not found on the bedrock at locs. 3 or 4 (Fig. 3; Table 2). The M2 terrace surface is older than the N-Y eruption, because at loc. 3 the surface is overlain by loess containing N-Y cryptotephra (MIS 4) (Fig. 3). The M2 terrace surface may be younger than MIS 5.2–5.3, MIS 5.1, because at loc. 3 the surface is not overlain by Dks or N-N cryptotephras. But it cannot be determined whether Dks and/or N-N glass shards may have been washed away or chemically altered. The mineral assemblage and the refractive indices thus do not clearly show whether the loess deposits of loc. 3 included Dks and N-N tephras. Thus, the M2 terrace correlates with MIS 5.1 or MIS 5.3 (79 ka or 97 ka; Bassinot et al., 1994: Table 2).

Vertical velocity inferred from GPS data

We used a set of daily site coordinates monitored by the 28 GPS stations to calculate the vertical velocities across the fore- and backarcs (Fig. 5A, Table 3). Figure 5B shows a representative time series of daily site coordinates, in which both seasonal changes (Heki, 2001, 2004b), which have constant periods, and long-term deformation can be clearly observed. Some of the GPS stations have a data gap corresponding to the occurrence of an earthquake or antenna replacement. We omitted data captured immediately after each seismic event or antenna replacement from our analysis.

In the forearc, the time series of stations 950176 (n: Wakuya) and 960549 (p: Yamoto) were affected by an earthquake of 26 July 2003 (Mj=6.2). These stations are on the hanging wall of a blind reverse fault underlying the Asahiyama flexure, and the coordinates show coseismic uplift (Miura et al., 2004). The antenna of station 950716 (n) was replaced on 17 July 2003, 9 days before the earthquake. Thus, the transient uplift after the earthquake includes a vertical component due to the antenna replacement. Stations 950175 (m: Shizugawa) and 950173 (e: Kurikoma) show transient uplift just after antenna replacement (16 July 2003). These uplifts are not due to the earthquake of 26 July 2003, because these stations are far from the earthquake-generating fault. Thus, for these stations, data from 21 March 1996 to 20 March 2002 (6 years) were employed in the analysis to obtain the vertical velocities by linear least-squares fitting (Fig. 5B, Table 3).

The time series of stations 950168 (a: Hanamaki), 940029 (c: Mizusawa 1), 960545 (d: Iwatekawasaki), 950174 (f: Naruko), 960548 (g: Shikama), 950169 (h: Tono), 950170 (i: Kamaishi), 960546 (j: Sumita), 950171 (k: Ofunato), 95172 (l: Kesennuma), 940036 (o: Onagawa), and 960549 (p: Yamoto) show transient deformation between the earthquake of 3 November 2002 (M=6.1) and that of 26 May 2003 (M=7.0). These apparent deformations were not coseismic but were due to antenna replacement. Thus, for these 12 stations, the date ranges used for data analysis were listed in Table 3. The time series of station 970796 (b: Isawa) showed a deformation pattern that changed from nearly flat to gradual subsidence without any transient deformation on the date of antenna replacement (10 May 2003). Thus, vertical velocities at this station were obtained by linear least-squares fitting of the data for the 5 years from 28 February 1998 to 27 February 2003 and 8 years from 28 February 1998 to 27 February 2006 (Fig. 5B, Table 3).

In the backarc, the time series of stations 960554 (10: Yuzawa), 950193 (11: Minase) and 940033 (12: Yamagatashinjo) indicate gradual uplift without any transient deformation. For station 960554 (10), and others, the data from 31 March 1997 to 30 March 2002, and 21 March 1996 to 20 March 2002 were employed in the analysis to obtain the vertical velocities by linear least-squares fitting (Fig. 5B, Table 3). Other stations, except for these three, show transient uplifts in the time series. However, no earthquakes capable of causing surface deformation (M>6.0) have been reported since 1997 in the backarc. Therefore, these apparent deformations are not coseismic but are due to antenna replacement, because in each case they occurred the day after antenna replacement. Thus, for stations 960544 (8: Yuda), we used data from 28 April 1997 to 27 April 2002, and for the others, data from 21 March 1996 to 20 March 2002 (Fig. 5B, Table 3).

The vertical velocities obtained at each station by linear least-squares fitting are summarized in Table 3. They range between −5.4±0.4 and 0.8±0.4 mm yr^{-1} in the forearc and between −3.1±0.3

Table 2
Terrace ages, paleo-shoreline parameters, and calculated uplift rates

Location	Terrace	MIS	Age (ka)	Height (m)	Difference between eustatic sea level and present sea level (m)	Uplift rate (m ka^{-1})
Iwaizaki	M1	5.5	122	16	+3	0.11
	M2	5.3	97	8	−10	0.19
	M2	5.1	79	8	−5	0.16
Myojinzaki	M1	5.5	122	20	+3	0.14

https://doi.org/10.1016/j.yqres.2008.12.005 Published online by Cambridge University Press

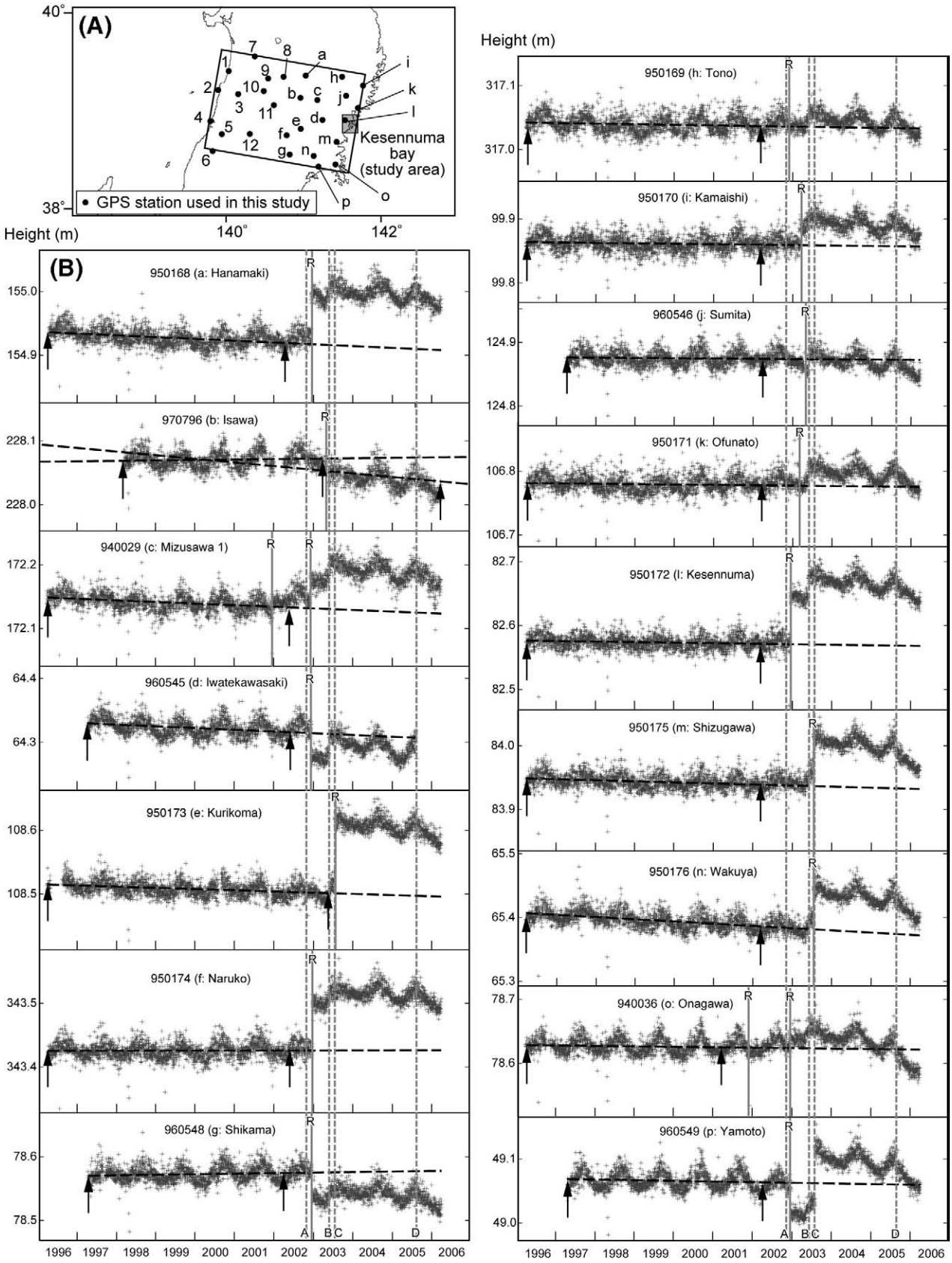

Figure 5. Short-term vertical velocities inferred from GPS observation data. (A) Map showing the distribution of GPS stations used in this study. Stations designated by letters are in the forearc, and numbered stations are in the backarc. (B) An example of a time series with fitted lines. The data set used for each fitted line is shown by paired arrows. Vertical dashed lines labeled A, B, C, and D indicate the earthquakes of 3 November 2002, 26 May 2003, 26 July 2003, and 16 August 2005, respectively. Solid vertical lines labeled R indicate dates of antenna replacement.

https://doi.org/10.1016/j.yqres.2008.12.005 Published online by Cambridge University Press

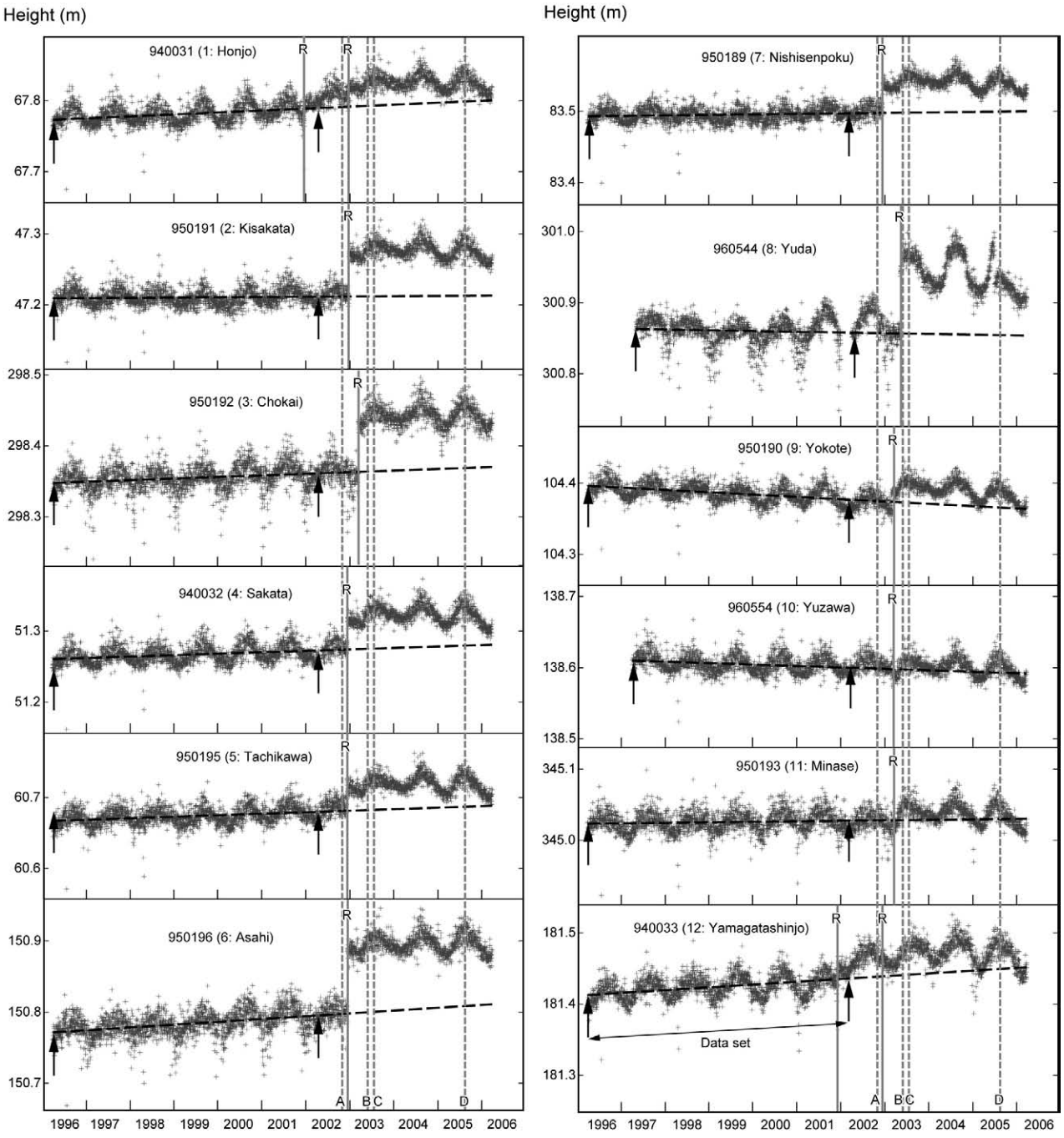

Figure 5 (*continued*).

and 4.0 ± 0.4 mm yr^{-1} in the backarc. In general, forearc stations show subsidence, whereas backarc stations show uplift. This specific pattern of vertical deformation is in good agreement with the results of previous studies (Danbara, 1971; Kato, 1979; Miura et al., 1989; El-Fiky and Kato, 1999; Aoki and Scholz, 2003; Suwa et al., 2006).

Discussion

Vertical velocity profile across the NE Japan forearc

The M1 and M2 terraces originated as wave-cut benches because neither terrace contains marine sediments (Fig. 3). These terrace surfaces without deposits are in accordance with the distribution of the present (Holocene) benches. The M1 terrace surface is overlain by Dks (MIS 5.3–5.2), N-N (MIS 5.2–5.1), and N-Y (MIS 4) cryptotephras, and the M2 terrace surface only by N-Y. Thus, the M1 and M2 terrace surfaces probably date to MIS 5.5 and MIS 5.3 or 5.1 (Table 2). According to Stirling et al. (1998: Table 2), eustatic sea levels during MIS 5.5, 5.3, and 5.1 were +3 m, −10 m, and −5 m relative to the present sea level.

Cross-sections of the M1 and M2 terrace surfaces are shown in Figure 6. We inferred an uplift rate of 0.11–0.19 m ka^{-1}. This rate is slightly lower than the reported rate of 0.14–0.23 m ka^{-1} (Koike and Machida, 2001) for uplift in this area, probably because we calculated the rate only from marine terrace surfaces, whereas Koike and Machida (2001) used the elevations of fluvial terrace surfaces as well.

Crustal uplift rates in the interior of the NE Japan forearc (Isawa upland: Fig. 1C) have been estimated from the relative heights of

https://doi.org/10.1016/j.yqres.2008.12.005 Published online by Cambridge University Press

Table 3
GPS station locations, antenna change dates, periods covered by each data set used in the analysis, and vertical velocities

Reference ID	Station ID	Station name	Latitude	Longitude	Height (m)	Data set	Vertical velocity (mm yr^{-1})	Standard error (99% confidence interval)	Antenna change
4	940032	Sakata	38.8946	139.8089	51.28	21 Mar. 1996–20 Mar. 2002	2.0	0.4	12 Dec. 2002
6	950196	Asahi	38.5940	139.8318	150.80	21 Mar. 1996–20 Mar. 2002	4.0	0.4	11 Dec. 2002
2	950191	Kisakata	39.2061	139.9077	47.21	21 Mar. 1996–20 Mar. 2002	0.4	0.4	24 Dec. 2002
5	950195	Tachikawa	38.7597	139.9574	60.69	21 Mar. 1996–20 Mar. 2002	2.1	0.5	7 Dec. 2002
1	940031	Honjo	39.3987	140.0482	67.78	21 Mar. 1996–20 Mar. 2002	2.7	0.4	20 Dec. 2001, 25 Dec. 2002
3	950192	Chokai	39.1642	140.1620	298.36	21 Mar. 1996–20 Mar. 2002	2.2	0.4	10 Mar. 2003
12	940033	Yamagatashinjo	38.7586	140.3187	181.43	21 Mar. 1996–20 Mar. 2002	3.9	0.4	5 Dec. 2001, 13 Dec. 2002
7	950189	Nishisenpoku	39.5493	140.3866	83.50	21 Mar. 1996–20 Mar. 2002	0.7	0.4	14 Dec. 2002
10	960554	Yuzawa	39.1991	140.5067	138.61	31 Mar. 1997–30 Mar. 2002	−2.0	0.4	9 Mar. 2003
9	950190	Yokote	39.3270	140.5598	104.37	21 Mar. 1996–20 Mar. 2002	−3.1	0.3	11 Mar. 2003
11	950193	Minase	39.0519	140.6296	345.03	21 Mar. 1996–20 Mar. 2002	0.9	0.4	11 Mar. 2003
8	960544	Yuda	39.3513	140.7692	300.86	28 Apr. 1997–27 Apr. 2002	−1.0	0.4	9 May 2003
f	950174	Naruko	38.7489	140.8016	343.43	26 Mar. 1996–25 Mar. 2002	0.1	0.4	21 Dec. 2002
g	960548	Shikama	38.5462	140.8479	78.57	31 Mar. 1997–30 Mar. 2002	0.8	0.4	14 Dec. 2002
b	970796	Isawa	39.1270	140.9885	228.07	28 Feb. 1998–27 Feb. 2003	0.8	0.3	10 May 2003
						28 Feb. 1998–27 Feb. 2006	−5.4	0.4	
e	950173	Kurikoma	38.8153	140.9906	108.50	21 Mar. 1996–20 Mar. 2003	−2.0	0.4	16 Jul. 2003
a	950168	Hanamaki	39.3626	141.0545	154.93	5 Apr. 1996–4 Apr. 2002	−2.8	0.5	11 Dec. 2002
n	950176	Wakuya	38.5395	141.1475	65.38	21 Mar. 1996–20 Mar. 2002	−3.6	0.5	17 Jul. 2003
c	940029	Mizusawa1	39.1106	141.2039	172.13	21 Mar. 1996–20 Mar. 2002	−2.5	0.4	12 Dec. 2001, 4 Dec. 2002
p	960549	Yamoto	38.4251	141.2129	49.10	31 Mar. 1997–30 Mar. 2002	−1.0	0.5	16 Dec. 2002
d	960545	Iwatekawasaki	38.9003	141.2748	64.33	30 Mar. 1997–29 Mar. 2002	−2.7	0.8	12 Dec. 2002
o	940036	Onagawa	38.4492	141.4412	78.60	21 Mar. 1996–20 Mar. 2001	−0.9	0.5	28 Nov. 2001, 18 Dec. 2002
m	950175	Shizugawa	38.6827	141.4494	83.94	21 Mar. 1996–20 Mar. 2002	−1.7	0.5	17 Jul. 2003
h	950169	Tono	39.3381	141.5342	317.04	21 Mar. 1996–20 Mar. 2002	−0.9	0.5	10 Dec. 2002
l	950172	Kesennuma	38.9029	141.5726	82.58	21 Mar. 1996–20 Mar. 2002	−0.8	0.6	12 Dec. 2002
j	960546	Sumita	39.1431	141.5755	124.88	31 Mar. 1997–30 Mar. 2002	−0.4	0.5	6 May 2003
k	950171	Ofunato	39.0238	141.7398	106.79	25 Mar. 1996–24 Mar. 2002	−0.6	0.6	12 Mar. 2003
i	950170	Kamaishi	39.2535	141.7980	99.86	21 Mar. 1996–20 Mar. 2002	−0.7	0.3	13 Mar. 2003

late Quaternary fluvial fill terrace surfaces (Matsu'ura et al., 2008) as 0.15–0.19±0.07 m ka^{-1} (Figs. 1B, 7A, B). This rate is nearly equal to, or slightly higher than, the uplift rate along the Pacific coast. Late Quaternary vertical velocities across the NE Japan forearc are thus nearly uniform, at about 0.11–0.19 m ka^{-1}, or increase slightly toward the interior. This long-term velocity profile (Fig. 7B) differs from the short-term vertical deformation profile in both direction and rate (Fig. 7C).

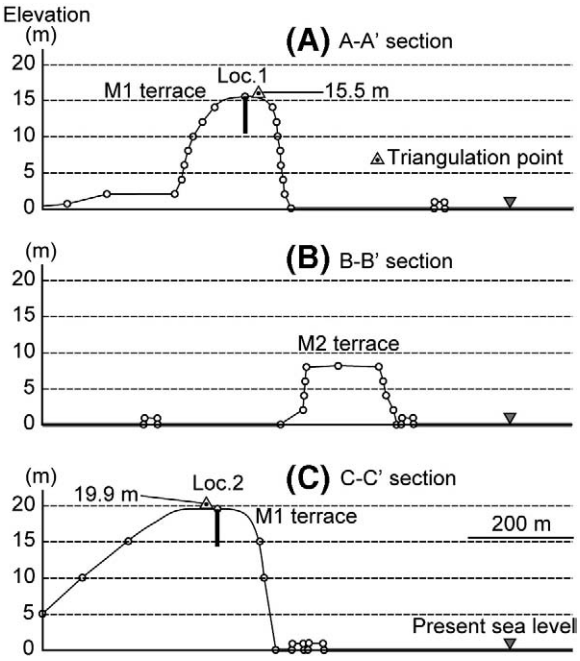

Figure 6. Profiles of marine terrace surfaces and the late Quaternary uplift rate. Locations of sections are shown in Figure 2. Triangulation points maintained by GSI are also shown.

Mechanism of forearc deformation in an erosion-dominant subduction zone

The short-term (geodetic) vertical deformation across the NE Japan arc shows forearc subsidence and backarc uplift (Fig. 7C). The hinge line (vertical velocity=0) is at the boundary between the forearc and the backarc. Subsidence in the coastal and inland areas was from 0 to −1.7 and from −2.0 to −5.4 mm yr^{-1}, respectively. Not only does this short-term subsidence contrast with the long-term uplift (Fig. 7B) in direction, but also the rate of the subsidence is nearly one order of magnitude higher than that of the long-term uplift. Thus, the forearc subsidence cannot be extrapolated to long-term tectonic movement. Short-term subsidence is probably driven by subduction erosion (Heki, 2004a) or elastic deformation caused by interplate coupling between the Pacific and the Eurasian plates, or both.

However, the long-term uplift requires a different explanation. Ikeda (1996) assumes that the forearc subsidence changed to uplift as a result of a large subduction zone moment release—that is, Armageddon faulting. In the Kuril subduction zone, a 17th century shallow coseismic rupture at −15 to −55 km did not cause uplift along the Pacific coast, and a deep afterslip at −55 to −85 km caused only transient uplift (Sawai et al., 2004). If the NE Japan forearc uplift was caused by Armageddon faulting, vertical deformation due to the faulting can be calculated by using a dislocation model (Mansinha and Smylie, 1971). Fault dip angles of deep and shallow parts were determined as 28.80° and 14.30° by Nakajima et al. (2001: Fig. 7D). According to the dislocation model calculations, a mega-thrust reaching 100 km depth (or more) would be required to cause nearly uniform uplift of the NE Japan forearc (Fig. 7E). Therefore, although the continental mantle, which is a viscoelastic material (in which moment releases rarely occur), might experience transient uplift driven by

https://doi.org/10.1016/j.yqres.2008.12.005 Published online by Cambridge University Press

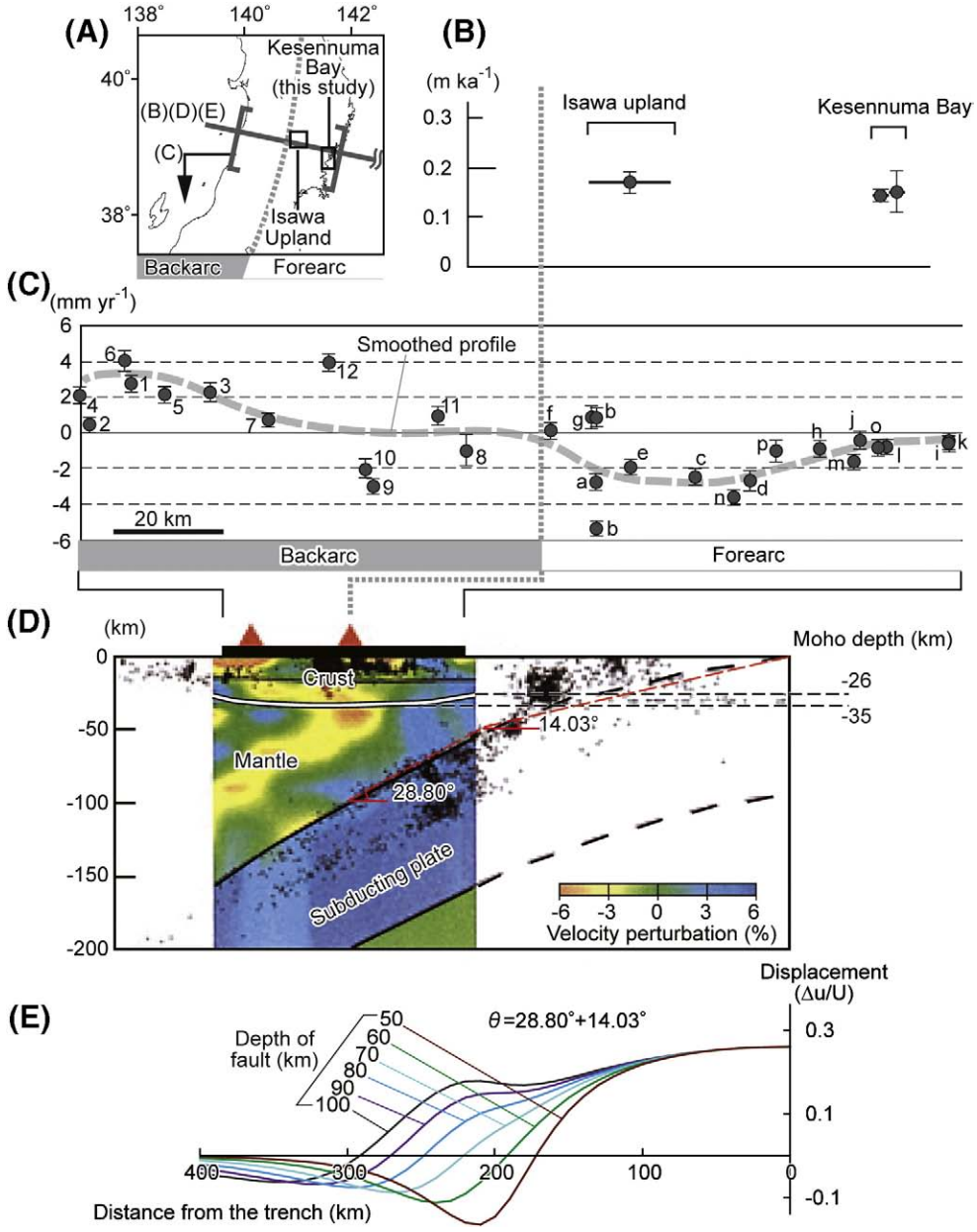

Figure 7. Long-term and short-term profiles of vertical velocities across the NE Japan arc. (A) Locations of sections across the central part of NE Japan. (B) Long-term late Quaternary uplift rates. (C) Profile of short-term vertical deformation obtained from GPS data. The standard error (99% confidence interval) of each vertical deformation rate is also shown. The vertical velocities in the forearc show subsidence, whereas those in the backarc show uplift, with the hinge line (vertical velocity=0) running along the middle of the NE Japan arc. This specific pattern of vertical deformation is in good agreement with results of previous studies. (D) Cross-section of P-wave velocity perturbations across the NE Japan arc. The image is from Nakajima et al. (2001), and Moho depths are from Nakajima et al. (2002). Red and blue velocity perturbations represent low and high velocities, respectively. The red triangles represent volcanoes, and the black dots indicate moment release values. Fault dip angles of the mega-thrust are also shown. (E) Vertical displacements of the ground surface in relation to fault depth. Δu/U is vertical displacement (Δu) normalized to the dip slip of the fault (U). Shallow (14.03° at ~50 km depth) and deep (28.80° at 50–100 km depth) fault dip angles were used to calculate the vertical displacements.

moment release on a mega-thrust, moment release probably cannot account for the long-term uplift of the NE Japan forearc.

In the Cascadia subduction zone (a sediment accretion-dominant zone), the long-term forearc uplift has been interpreted as driven by both accretion and within-wedge deformation (Brandon et al., 1998). The long-term uplift of the Cascadia forearc, shown by upstream divergence of fluvial terrace surfaces, is in accordance with the short-term uplift in direction (Pazzaglia and Brandon, 2001). This long-term uplift rate (implied by the incision rate) is an order of magnitude lower than the short-term uplift rate (Pazzaglia and Brandon, 2001), probably because the long-term uplift does not include elastic deformation caused by an earthquake cycle, given that the Cascadia subduction thrust is locked (Fleymuller et al., 2000). But because the NE Japan arc, which is in an erosion-dominant subduction zone, lacks thick accretionary deposits under the forearc (von Huene and Scholl, 1991; Heki, 2004a), this explanation for the long-term forearc uplift in the Cascadia subduction zone is not applicable to the NE Japan forearc.

Under the NE Japan forearc, the Moho depth is 26 km beneath the Pacific coast and 35 km beneath the interior arc (Fig. 7D: Nakajima et al., 2002). Thus, the crust thickens from the trench toward the interior of the arc. Low-velocity material, which implies hot mantle material from depth, ascends to the bottom of the crust (Fig. 7E) and probably underplates the crust, causing crustal thickening. The long-term vertical velocity profile is in accordance with the Moho depth profile if the slow and constant uplift of the NE Japan forearc is attributed to tectonic uplift, such as isostatic uplift driven by crustal thickening.

https://doi.org/10.1016/j.yqres.2008.12.005 Published online by Cambridge University Press

Although it is still uncertain whether crustal thickening can cause effective isostatic uplift in subduction zones, this possibility should be investigated further by determining late Quaternary vertical velocities across the whole NE Japan arc (fore- and backarc).

Conclusion

We inferred the uplift rate of the central part of the NE Japan forearc, the overriding plate in the NE Japan subduction zone, from late Quaternary marine terraces. Marine terraces in Kesennuma Bay were correlated with MISs by tephrochronology. Our conclusions are as follows:

(1) We classified the terrace surfaces as M1 and M2 and L1 and L2, in descending order. M1 and M2 are marine terraces and date to MIS 5.5 and MIS 5.1 (or MIS 5.3), respectively.
(2) Uplift rates, obtained from the relative heights of the late Quaternary terrace surfaces and paleo-sea levels, were 0.11–0.19 m ka^{-1}. The long-term vertical velocity profile across the NE Japan forearc, as shown by marine and fluvial terrace surfaces, revealed nearly uniform, or slightly increasing, uplift toward the interior at the rate of 0.15–0.19 m ka^{-1}.
(3) The long-term (geological) uplift is inconsistent with the short-term (geodetic) subsidence in the NE Japan forearc, so the short-term tectonic movements cannot be extrapolated to long-term movements. Furthermore, the NE Japan forearc uplift, which is occurring in an erosion-dominant subduction zone, is different from that in the Cascadia forearc, which is in a sediment accretion-dominant zone and is driven by both accretion and within-wedge deformation. Isostatic uplift driven by crustal thickening in this erosion-dominant subduction zone is likely, as suggested by the Moho depth profile, but this possibility should be investigated further by determining late Quaternary vertical velocities across the whole NE Japan arc (fore- and backarc).

Acknowledgments

We thank K. Otsuki, S. Kanisawa (Tohoku University), T. Oguchi (University of Tokyo), T. Komatsubara, K. Satake, I. Miyagi, J. Itoh, Y. Namegaya, H. Horikawa (Geological Survey of Japan), T. Yoshiki (Iwate Prefectural University), B. Miyahara and M. Koarai (Geographical Survey Institute) for their constructive comments. We benefited from the comments of B. Sherrod (US Geological Suurvey) and K. Heki (Hokkaido University) which improved the manuscript. We used the code of calculation of dislocation by T. Komatsubara.

References

Altamimi, Z., Sillard, P., Boucher, C., 2002. ITRF2000: a new release of the International Terrestrial Reference Frame for earth science applications. Journal of Geophysical Research 107, doi:10.1029/2001JB000561.
Aoki, Y., Scholz, C.H., 2003. Vertical deformation of the Japanese islands 1996–1999. Journal of Geophysical Research 108, 2257, doi:10.1029/2002JB002129.
Bassinot, F.C., Labeyrie, L.D., Vincent, E., Quidelleur, X., Shackleton, N.J., Lancelot, Y., 1994. The astronomical theory of climate and the age of the Brunhes–Matuyama magnetic reversal. Earth and Planetary Science Letters 126, 91–108.
Brandon, M.T., Roden-Tice, M.K., Garver, J.I., 1998. Late Cenozoic exhumation of the Cascadia accretionary wedge in the Olympic Mountains, northwest Washington State. Geological Society of America Bulletin 110, 985–1009.
Danbara, T., 1971. Synthetic vertical movements in Japan during the recent 70 years. Journal of the Geodotic Society of Japan 17, 100–108 (in Japanese with English abstract).
El-Fiky, G.S., Kato, T., 1999. Interplate coupling in the Tohoku district, Japan, deduced from geodetic data inversion. Journal of Geophysical Research 102, 20539–20550.
Fitch, T.J., Scholz, C.H., 1971. Mechanism of underthrusting in southwest Japan: a model of convergent plate interactions. Journal of Geophysical Research 76, 7260–7292.
Fleymuller, J.Y., Cohen, S.C., Fletcher, H.J., 2000. Spatial variations in present-day deformation, Kenai Peninsula, Alaska, and their implications. Journal of Geophysical Research 105, 8079–8101.
Furusawa, A., 1995. Identification of tephra based on statistical analysis of refractive index and morphological classification of volcanic glass shards. Journal of the Geological Society of Japan 101, 123–133 (in Japanese with English abstract).
Hatanaka, Y., Iizuka, T., Sawada, M., Yamagiwa, A., Kikuta, Y., Johnson, M., Rocken, C., 2003. Improvement of the analysis strategy of GEONET. Bulletin of the Geographical Survey Institute 49, 11–37.
Heki, K., 2001. Seasonal modulation of interseismic strain buildup in Northeastern Japan driven by snow loads. Science 293, 89–92.
Heki, K., 2004a. Space geodetic observation of deep basal subduction erosion in northeastern Japan. Earth and Planetary Science Letters 219, 13–20.
Heki, K., 2004b. Dense GPS array as a new sensor of seasonal changes of surface loads. In: Sparks, R.S.J., Hawkesworth, C.J. (Eds.), The State of the Planet: Frontiers and Challenges in Geophysics. Geophys. Monograph, 150. American Geophysical Union, Washington, pp. 177–196.
Hyndman, R.D., Wang, K., 1995. The rupture zone of Cascadia great earthquakes from current deformation and the thermal regime. Journal of Geophysical Research 100, 22133–22154.
Ikeda, Y., 1996. Implication of active fault study for the present-day tectonics of the Japan arc. Active Fault Research 15, 93–99 (in Japanese with English abstract).
Kato, T., 1979. Crustal movements in the Tohoku district, Japan, during the period 1900–1975, and their tectonic implications. Tectonophysics 60, 141–167.
Koike, K., Machida, H., 2001. Atlas of Quaternary Marine Terraces in the Japanese Islands. University of Tokyo Press, Tokyo. (in Japanese with English abstract).
Machida, H., Arai, F., 2003. Atlas of Tephra in and Around Japan. University of Tokyo Press, Tokyo. 336 pp. (in Japanese with English abstract).
Maemoku, H., Tsubono, K., 1990. Holocene crustal movements in the southern part of Kii Peninsula, outer zone of southwest Japan. Journal of Geograhy 99, 349–369 (in Japanese with English abstract).
Mansinha, L., Smylie, D.E., 1971. The displacement fields of inclined faults. Bulletin of the Seismological Society of America 61, 1433–1440.
Matsu'ura, T., Nitta, E., Kanisawa, S., Nakashima, K., 2002. Dokusawa tephra erupted at approximately 100 ka and its eruptive process in the central part of northeast Japan. Bulletin of the Volcanological Society of Japan 47, 711–725 (in Japanese with English abstract).
Matsu'ura, T., Nitta, E., Kanisawa, S., Nakashima, K., 2003. Correlation of Dokusawa and Kitahara tephras in the central part of Northeast Japan—EPMA analyses of heavy minerals. Science Reports of Tohoku University, 7th Series (Geography) 52, 29–44.
Matsu'ura, T., Furusawa, A., Saomoto, H., 2008. Late Quaternary uplift rate of the northeastern Japan arc inferred from fluvial terraces. Geomorphology 95, 384–397, doi:10.1016/j.geomorph.2007.06.011.
Miura, O., 1966. Coastal terraces and rias along the Kesennuma Bay, Miyagi Prefecture. Annals of the Tohoku Geograhical Association 18, 116–122 (in Japanese with English abstract).
Miura, D., Ishii, H., Takagi, A., 1989. Migration of vertical deformations and coupling of island arc plate and subducting plate. Geophys. Monogr. 49, 125–138 Slow deformation and transmission of stress in the earth. American Geophysical Union.
Miura, S., Suwa, Y., Sato, T., Tachibana, K., Hasegawa, A., 2004. Slip distribution of the northern Miyagi earthquake (M6.4) deduced from geodetic inversion. Earth Planets Space 56, 95–101.
Nakajima, J., Matsuzawa, T., Hasegawa, A., Zhao, D., 2001. Three-dimensional structure of Vp, Vs, and Vp/Vs beneath northeastern Japan: implications for arc magmatism and fluids. Journal of Geophysical Research 106, 21843–21857.
Nakajima, J., Matsuzawa, T., Hasegawa, A., 2002. Moho depth variation in the central part of northeastern Japan estimated from reflected and converted waves. Physics of the Earth and Planetary Interiors 130, 31–47.
Pazzaglia, F.J., Brandon, M.T., 2001. A fluvial record of long-term steady-state uplift and erosion across the Cascadia forearc high, western Washington state. American Journal of Science 301, 385–431.
Plafker, G., 1972. Alaskan earthquake of 1964 and Chilean earthquake of 1960: implications for arc tectonics. Journal of Geophysical Research 77, 901–925.
Plafker, G., 1987. Application of marine-terrace data to paleoseismic studies. In: Crone, A.J., Omdahl, E.M. (Eds.), Directions in Paleoseismology. United States Geological Survey Open—file Report 87–673, pp. 146–156.
Research Group for Active Faults of Japan, 1991. Active Faults in Japan: Sheet Maps and Inventories(revised edition). University of Tokyo Press, Tokyo. 437 pp. (in Japanese with English abstract).
Satake, K., Wang, K., Atwater, B.F., 2003. Fault slip and seismic moment of the 1700 Cascadia earthquake inferred from Japanese tsunami descriptions. Journal of Geophysical Research 108, B11, doi:10.1029/2003JB002521.
Savage, J.C., Thatcher, W., 1992. Interseismic deformation at the Nankai Trough, Japan, subduction zone. Journal of Geophysical Research 97 (B7), 11117–11135.
Sawai, Y., Satake, K., Kamataki, T., Nasu, H., Shishikura, M., Atwater, B.F., Horton, B.P., Kelsey, H.M., Nagumo, T., Yamaguchi, M., 2004. Transient uplift after a 17th-century earthquake along the Kuril subduction zone. Science 306, 1918–1920.
Soda, T., 1989. Tephrochronological study of the layers including the early Paleolithic artifacts in the northern part of Sendai plain. Quartenary Research (Japan) 28, 269–282 (in Japanese with English abstract).
Soda, T., 1996. Pyroclastic flow deposits and air-fall tephras erupted from the Naruko caldera. Japan Association for Quaternary Research ed. Inventory of Quaternary Outcrops—Tephras in Japan. Japan Association for Quaternary Research 40th anniversary special publication 156 (in Japanese).
Stirling, C.H., Esat, T.M., Lambeck, K., McCulloch, M.T., 1998. Timing and duration of the last interglacial: evidence for a restricted interval of widespread coral reef growth. Earth and Planetary Science Letters 160, 745–762.
Suwa, Y., Miura, S., Hasegawa, A., Sato, T., Tachibana, K., 2006. Interplate coupling beneath NE Japan inferred from three-dimensional displacement field. Journal of Geophysical Research 111, B04402, doi:10.1029/2004JB003203.

Tsuchiya, N., Itoh, J., Seki, Y., Iwaya, T., 1997. Geology of the Iwagasaki district. With Geological sheet map at 1:50,000, Geological Survey of Japan, 96 pp. (in Japanese with English abstract).
von Huene, R., Scholl, D., 1991. Observations at convergent margins concerning sediment subduction, subduction erosion, and the growth of continental crust. Review of Geophysics 29, 279–316.
Wang, K., Wells, R., Mazzotti, S., Hyndman, R.D., Sagiya, T., 2003. A revised dislocation model of interseismic deformation of the Cascadia subduction zone. Journal of Geophysical Research 108 (B1), 2026, doi:10.1029/2001JB001227.
Yokoyama, R., Shirasawa, M., Pike, R., 2002. Visualizing topography by openness: a new application of image processing to digital elevation models. Photogrammetric Engineering and Remote Sensing 68, 257–265.
Yoshikawa, T., Kaizuka, S., Ota, Y., 1964. Mode of crustal movement in the late Quaternary on the southeast coast of Shikoku, southwestern Japan. Geographical Review of Japan 37, 627–648 (in Japanese with English abstract).
Zong, Y., Shennan, I., Combellick, R.A., Hamilton, S.L., Rutherford, M.M., 2003. Microfossil evidence for land movements associated with the AD 1964 Alaska earthquake. Holocene 13, 7–20.